Ternary nanocomposite potentiates the lysophosphatidic acid effect on human osteoblast (MG63) maturation

Hoda Elkhenany[1*], Mohamed Abd Elkodous[2,] and Jason Peter Mansell[3*]

[1] Department of Surgery, Faculty of Veterinary Medicine, Alexandria University, Alexandria 22785, Egypt.

[2] Department of Electrical and Electronic Information Engineering, Toyohashi University of Technology, 1-1 Hibarigaoka, Tempaku-Cho, Toyohashi, Aichi 441-8580, Japan

[3]Department of Applied Sciences, the University of the West of England, Frenchay Campus, Coldharbour Lane, Bristol BS16 1QY, UK

*Correspondence: hoda.atef@alexu.edu.eg (Elkhenany H), jason.mansell@uwe.ac.uk (Mansell JP).

Acknowledgment

Hoda Elkhenany would like to acknowledge the British Academy of Medical Sciences for the financial support of her visit to the Department of Applied Sciences, the University of the West of England, Bristol, UK through a Daniel Turnberg Travel Fellowship.

Abstract

Aim: This study aimed to investigate the potential of ternary nanocomposite (TNC) to support MG63 osteoblast maturation to EB1089-FHBP co-treatment.

Materials & methods: Binary (P25/rGO) nanocomposite was prepared, and Ag NPs were loaded onto the surface to form TNC (P25/rGO/Ag). The influence of TNC on proliferation, alkaline phosphatase (ALP) activity, osteogenic gene expressions were evaluated in a model of osteoblast maturation wherein MG63 are co-stimulated with EB1089 and FHBP.

Results: TNC has no cytotoxic effect on MG63's. The inclusion of TNC to EB1089-FHBP co-treatment, enhanced the maturation of MG63 as supported by the greater ALP activity, OPN and OCN gene expression.

Conclusion: TNC acts as a promising carrier for FHBP, composite which may find an application in bone regenerative setting.

Plain language summary: Our study explored the potential of a ternary nanocomposite (TNC) for bone cell development and regeneration. TNC, formed by combining P25/rGO nanocomposite with silver nanoparticles (Ag NPs), was tested on MG63 osteoblast-like cells. The results showed that TNC is safe for these cells and does not cause any toxicity. Additionally, when TNC was used in combination with EB1089 and FHBP, it enhanced the maturation of MG63 cells, as indicated by increased alkaline phosphatase (ALP) activity and the expression of osteopontin (OPN) and osteocalcin (OCN) genes. This suggests that TNC has the potential to support the development of mature bone cells. In conclusion, TNC could serve as a promising carrier for FHBP, opening up possibilities for its application in bone regeneration.

Keywords: Bone regeneration, Drug delivery, Osteoblast maturation, Reduced graphene, Titanium dioxide nanoparticles

Promoting bone healing and regeneration following the application of bone void fillers and/or endoprostheses are highly desirable. One way in which this could be realised is to enhance the maturation of bone-forming osteoblasts. Biomaterial coatings and/or the controlled local delivery of suitable agents may have the potential to augment overall bone healing and health in this setting.

Lysophosphatidic acid (LPA) is a product of platelet activation with growth-factor-like activities and considered an important mediator of tissue repair and regeneration [1]. In our laboratory, we have harnessed the potential of the LPA analog ((3S)1-fluoro-3-hydroxy-4-(oleoyloxy) butyl-1-phosphonate, FHBP) in combination with calcitriol (1,25D) to enhance human osteoblast (MG63) maturation [2-4]. We recently reported on the successful, facile coating of titanium (Ti) with FHBP to enhance 1,25D-induced osteoblast maturation [3].

Nanotechnology is proving to provide a valuable contribution to tissue engineering and regenerative medicine. Refining the quality of the engineered tissue depends mainly on the microenvironment and, where applicable, the longevity of selected growth factors (GF) through what is called nanoreservoir technology [5, 6]. For example, a polycaprolactone (PCL) bio-membrane functionalized with BMP-2 and ibuprofen stimulates osteogenesis in maxillary bone defects [7]. Also, loading or encapsulating the herbal extracts in the nanoform such as propolis or curcumin has shown a positive contribution to skin and spinal cord regeneration [8-10]. Furthermore, nanoparticles without biological functionalization have shown to enhance cell proliferation and differentiation. For instance, reduced graphene oxide (rGO) has been shown to induce and enhance osteogenic differentiation of adult mesenchymal stem cells (MSCs) *in vitro* and *in vivo* [11, 12]. Of particular relevance to LPA is the very recent report that graphene oxide forms strong hydrogen bonds with LPA in nanoseconds (Liu et al. 2022). The resultant complex was able to stimulate the hippo-yes associated protein (YAP) signalling pathway in endothelial tip cells. Given the structural similarities between LPA and FHBP it is highly probable that the latter agent will bond well to graphene oxide. Moreover, graphene nanocoatings provide superior long-lasting corrosion protection to Ti alloy [13]. Titanium dioxide (TiO_2), however, encompassed by the risk of cytotoxicity [14-16], has shown a profound regenerative capacity in topical applications for wound healing [17, 18]. There are conflicting reports regarding the influence of TiO_2 on bone tissue engineering. In nanotube form, TiO_2 efficiently fills a rodent femoral defect as well as enhancing osteoblast alkaline

phosphatase activity within 7 days [19]. Furthermore, a 3D bone spheroid treated with TiO_2 exhibited higher collagen deposition which is the main component of the bone ECM [20]. On the other hand, Niska K *et al* [21] have reported a negative impact of TiO_2 (5–15 nm) on hFOB 1.19 human osteoblast cells and this was confirmed by low alkaline phosphatase and superoxide dismutase (SOD) activity. As shown by Zhang Y *et al* [22], the TiO_2 cytotoxicity is largely correlated to the particle size which increases with small size particles. Taken together, the integration of TiO_2, at the optimal particle size and concentration, to composite or scaffold can provide suitable durability and mechanical strength and inhibits microbial infections [19, 23].

Furthermore, the continuing issue of aseptic loosening and infection of orthopaedic Ti implants [24], has created a need for broad-spectrum, long-acting antimicrobial coatings to enhance implant longevity [25]. Antimicrobial Silver nanoparticles (AgNPs) have been used to coat a variety of orthopaedic devices such as external fixation pins, proximal femur or tibia mega-prostheses and bone cement [26]. This effect was believed to be due to direct contact of the Ag with the microorganism and caused membrane damage and consequently death [27]. In addition, the sustained release of silver ions (Ag^+) from AgNPs can bind to specific proteins in the bacterial cell membrane and compromises them which consequently limits cell membrane permeability and function [28]. There is also clear evidence that Ag^+ can increase ROS production and cellular oxidative stress inside the microbe [29, 30].

As part of our ongoing programme to encourage bone healing following arthroplasty, we examined the potential of an FHBP-functionalised ternary nanocomposite (TNC) on MG63 maturation. The TNC comprises of TiO_2-reduced graphene doped with Ag NPs. Rather than use 1,25D to synergise with FHBP we utilised the potent and less calcaemic analog, EB1089 [31-33].

Materials and methods

Materials

Nitric acid (HNO_3), potassium chlorate ($KClO_3$), sulfuric acid (H_2SO_4), hydrochloric acid (HCl), P25 (TiO_2), absolute ethanol 99.9% (C_2H_5OH), ammonium hydroxide 25 % (NH_4OH), and silver nitrate ($AgNO_3$) were purchased from Sigma Aldrich, Germany.

133 Unless stated otherwise all reagents were from Sigma-Aldrich (Poole, UK). Dulbecco's
134 modified Eagle medium (DMEM)/ Ham's F12, fetal calf serum (FCS), and trypsin–
135 EDTA were obtained from Gibco (Paisley, Scotland). Stocks of (3S)1-fluoro-3-
136 hydroxy-4-(oleoyloxy)butyl-1-phosphonate (FHBP, 500 μM, Tebu-bio, Peterborough,
137 UK) was prepared in ethanol: tissue culture grade water (1:1) and stored at −20 °C.
138 Likewise, the 1,25D analog, EB1089 (Tocris Bioscience) was prepared in ethanol and
139 stored at −20 °C. Orthopaedic-grade Ti discs (Ti6AL4V, 10 mm diameter, thickness 2
140 mm) were kindly provided by Osteocare (Slough, UK). Tetrazolium compound 3-(4,5-
141 dimethylthiazol-2-yl)-5-(3-carboxymethoxy-phenyl)-2-(4-sulfophenyl)-2H-tetrazolium,
142 inner salt was obtained from Promega (Southampton, UK) and stored at 4°C.

143 **Preparation and characterization of TNC**

144 **Preparation of GO**

145 GO was prepared using a modified Staudenmaier's method [34]. Briefly, graphite
146 powder (5 g) was oxidized chemically in a mixture (135 mL) of nitric acid 68 % (45 mL)
147 and sulfuric acid 98 % (90 mL) (1:2 v/v). Then, the mixture was left to stir at room
148 temperature for (30 min) followed by cooling in an ice bath. After that, potassium
149 chlorate (55 g) was added to the mixture which was left under constant stirring for (5
150 days) until complete oxidation. Then, the obtained powder was washed frequently
151 using deionized water (D.I.W) until pH 7 was reached. Then 10 % hydrochloric acid
152 was used to remove any residual sulfate or other impurities (until a negative reaction
153 on sulfate and chloride ions was achieved by using $Ba(NO_3)_2$ and $AgNO_3$,
154 respectively). Finally, the resulted GO powder was vacuum dried at 60ºC for 48 h.

155 **Preparation of exfoliated rGO**

156 GO powder from the previous step was exfoliated into rGO powder with a large surface
157 area using the microwave-assisted method [35]. GO powder (1.5 g) was placed in an
158 alumina crucible and microwave irradiated, (900 W for 30 S) using IRIS OHYAMA,
159 Japan.

160 **Preparation of TNC**

161 First, P25 was loaded onto rGO nanosheets (15 % w/w with respect to P25) using a
162 simple impregnation method [36]. Calculated amounts of P25 (400 mg) and rGO (60
163 mg) were dispersed in absolute ethanol (45 mL) using ultrasonication for 45 min. Then,

164 1 ml of ammonia (25 % w/v) was added to the dispersion which was left under vigorous
165 stirring overnight. Finally, 5 wt.% Ag NPs (20 mg) were loaded onto P25 nanoparticles
166 using the ultraviolet (UV)-assisted photodeposition method. The corresponding
167 volume (10 mL) of silver nitrate solution (2 mg/mL) was added to P25/rGO ethanol
168 dispersion which was irradiated by an HgXe lamp (275 W, SP-11, USHIO, Japan),
169 operating at 275 W power and 100 % intensity for 30 min under N_2 bubbling. Finally,
170 the resulted powder was collected by centrifugation, washed with ethanol many times,
171 and finally dried under vacuum overnight.

172 **Characterization of the prepared TNC**

173 Phase and crystallinity were confirmed via X-ray diffraction (XRD) analysis on Ultima
174 IV (Rigaku, Japan) X-ray diffractometer, using Cu-Kα radiation (λ = 1.54 Å) and
175 operating at 30 mA - 40 kV. While morphology, the average size of particles, and their
176 distribution were revealed using scanning transmission electron microscopy (STEM)
177 by JEM-2100F (JEOL Ltd., Japan), supported by the JED-2300T EDS unit. Finally, the
178 stability of particles in different pH values (2, 7, and 11) was investigated by an ELS-
179 Z1NT analyzer (Photo OTSUKA ELECTRONICS, Japan).

180 **Preparation of TNC for cell culture**

181 A 10 mg/mL of TNC was prepared by dissolving the powder in 35 ml of 57% (v/v)
182 aqueous ethanol and ultrasonication for 30 min. Then 10 ml of tris base (25 mmol, PH
183 7.2) was added and stirred overnight at 25 °C. The mixture was then centrifuged at
184 5000 rpm for 15 min and the pellet was washed twice with water and resuspended in
185 1 ml serum-free DMEM/F12 (SFCM) for cell culture applications.

186 **Human osteoblast-like cell (MG63) culture**

187 MG63 Cells were maintained to confluence in DMEM/F12 containing L-glutamine (4
188 mM), sodium pyruvate (1 mM), 10% v/v FCS, streptomycin (20 μg/mL), penicillin (20
189 units/mL) and non-essential amino acids. At 80% confluency, MG63's was
190 subsequently seeded into 24-well plates at a cell seeding density of 2 x 10^4
191 cells/ml/well suspension. After 3 days of culture, cells were then cultured with SFCM
192 to starve the cells overnight. Osteoblasts were subsequently treated with EB1089 (100
193 nM), FHBP (2 μM), TNC (100 μg/mL final concentration) and their combinations.

194 *Coating tissue culture plastic (TCP) with FHBP and TNC using catecholamines.*
195 A preliminary experiment was conducted to compare the efficacy of 2
196 polycatecholamines, poly-dopamine (PDA) and poly-norepinephrine (PNE) to
197 functionalise 24 well TCP with FHBP. Next, we coated TCP with different combinations
198 of EB1089 (100 nM), FHBP (2 μM), and TNC (100 μg) with the aid of PDA [37]. Briefly,
199 each of the previous components at the defined concentrations were prepared in Tris
200 (10 mM, pH 8.8) which was subsequently combined with dopamine hydrochloride and
201 dispensed immediately into wells and kept at room temperature for 2 hours. After that,
202 the solutions were discarded, and the treated wells were washed twice with cell
203 culture-grade water followed by rinsing with serum-free DMEM/F12 (1 ml). Cells were
204 seeded directly to the treated wells at density of 1.2 x 10^5 cells/mL/well. Three days
205 later, ALP activity was evaluated as detailed below. Additionally, Alizarin red staining
206 was performed to assess the mineralization potential of the cells in the different
207 treatment combinations. Images of the cell morphological changes were taken.

208 **MTS/PMS assay to evaluate the TNC cytotoxicity and biocompatibility.**
209 MG63 cell viability was evaluated by a combination of MTS reagent (2 mg/mL) and
210 PMS (1 mg/mL) with a ratio of 19:1 MTS:PMS following the manufacturer's instructions
211 [38]. The culture medium was removed and replaced with fresh SFCM (500 μL/well)
212 and spiked with 100 μL of MTS/PMS reagent. The optical density was measured at
213 492 nm after 45 min incubation at 37 °C using a multi-plate reader. For determination
214 of the cell number, a stock suspension of MG63 cells (8.5 × 10^5 cells/ml) was serially
215 diluted in SFCM to give a series of known cell concentrations down to 25 × 10^3 cells/ml
216 to generate a standard curve.

217 **Alkaline phosphatase assay**

218 Quantitative analysis of MG63 ALP activity after treatments was measured as
219 described previously [39]. Following an incubation period of 3 days with different
220 treatment groups, the medium was removed, and the monolayers were lysed with 7
221 mM sodium carbonate/3 mM sodium bicarbonate (0.1 mL, pH 10.3), supplemented
222 with Triton X-100 (0.1% (v/v)). After 2 min each well was treated with 15 mM p-
223 nitrophenylphosphate (p-NPP) (di-tris salt, 0.2 mL) in 70 mM sodium carbonate/30 mM
224 sodium bicarbonate (pH 10.3) and supplemented with 1 mM $MgCl_2$. Lysates were then
225 incubated under conventional cell culture conditions (37 °C) for 50 min. After that, 0.1

226 mL aliquots were transferred to a 96-well plate and the absorbance read at 405 nm.
227 An ascending series of p-nitrophenol (p-NP) (50–400 μM) prepared in the substrate
228 buffer enabled quantification of product formation.

229 **FHBP-TNC binding study**

230 To investigate the binding of TNC with FHBP, we incubated the NPs suspension in
231 SFCM (15 ml) in the same concentration under investigation with FHBP for 1 hour on
232 a roller at room temperature. The suspension then was centrifuged at 5000 rpm for 15
233 min. The supernatant was decanted into a separate tube and the TNC pellet was
234 resuspended in SFCM (15 ml). Established monolayers of MG63 cells that were
235 starved for 24 hours were treated with supernatant and resuspended pellet alone or in
236 combination with EB1089 (100nM). Also, cells were treated with either EB1089, FHBP
237 (500nM), EB1089+FHBP, or EB1089+FHBP+ TNC as control groups (**Figure 5A**).

238 **mRNA gene expression using real-time quantitative polymerase chain reaction**
239 **(RT-qPCR)**

240 RNA was extracted from cells cultured for 3 days using the Quick-RNA™ MiniPrep kit
241 (cat. No. R1054, Zymo Research, USA) according to the manufacturer's instructions.
242 The cDNA was synthesized by using the QuantiTect® Reverse Transcription Kit
243 (QIAGEN, Germany) and a quantitative Real-Time PCR assay was performed using
244 PowerUp™ SYBR™ Green Master Mix (applied biosystems, Thermo Fisher Scientific,
245 Lithuania) on Step One Plus RT-PCR System (Applied Biosystems) using StepOne™
246 software v2.3. The sequences of the primers are identified in **Supplementary table1**.
247 The relative gene expression was calculated using the comparative threshold ($2^{\Delta\Delta CT}$)
248 method and the data were normalized to GAPDH gene expression.

249 **Coating Ti-discs with TNC**

250 Ti discs (10 mm diameter, 2 mm thick) were coated with TNC using the drop-casting
251 technique in which TNC (100 μg/100 μl) was dispensed onto the upper surface of the
252 disc and incubated at 60 °C for 1.5 hr or until completely dry. Another technique with
253 slight modification was used in which the TNC (100 μg/20 μl) was dispensed onto the
254 top of the disc and covered with parafilm, to ensure equal distribution of the NPs over

255 the disc surface. These discs were incubated at 37 °C for 1 hr. All the coated discs
256 were washed 3x using cell culture-grade water with strong shaking. MG63 cells (1 x
257 10^5 cells/ 100 µL) were dispensed onto the surface of the discs and incubated at 37 °C
258 in a humidified 5% CO_2 incubator for 1 hr to ensure cell adhesion to the Ti surface.
259 Once completed 1ml of SFCM was applied to each disc and the samples incubated
260 for 3 days prior to an assessment of cell proliferation using the MTS/PMS assay.
261 Surface wettability was measured before and after TNC treatment using the
262 Model 68-76 Pocket Goniometer PGX+ and PGX+ software (Testing Machines Inc.,
263 New Castle, Delaware, USA) as described before [37].
264
265 **Statistical analysis**
266 The experimental data were collected from three independent experiments, and the
267 results were reported as the mean ± standard deviation (SD). One-way ANOVA with
268 appropriate corrections (Tukey's post hoc test) was used to compare groups in
269 MTS/PMS, ALP assays, and RT-PCR. For the comparisons between two groups of
270 values, the statistical analysis of the results was performed using the student's t-test
271 for normally distributed data. Statistical analyses were performed using GraphPad
272 Prism version 9.0.0 (La Jolla, CA, USA). Significant differences were identified as
273 follows * $p < 0.05$, ** $p < 0.01$, *** $p < 0.001$, and **** $p < 0.0001$.
274
275 ## Results

276 **Characterization of TNC**

277 As shown in **Figure 1A**, many characteristic peaks were recorded in the XRD pattern
278 at 2θ = 25.3° (101), 27.5° (110), 35.7° (101), 36.2° (103), 37.2° (004), 37.8° (112),
279 41.5° (111), 47.5° (200), 52.6° (105), 54.4° (211), 63.8° (204), 69.8° (116), 71.58°
280 (220), 75.6° (215), and 75.9° (301). Those diffraction peaks and their corresponding
281 crystallographic planes were found to be in good agreement with the JCPDS card
282 number (21-1276) of the P25 [40]. While a characteristic (002) of carbon materials
283 appeared at 2θ = 26.25°. **Figure 1A** confirming the conjugation between rGO
284 nanosheets and P25. While **Figure 1B**, shows the characteristic XRD pattern of bare
285 rGO sheets. It is worth mentioning that characteristic XRD peaks of Ag NPs

disappeared due to their lower intensity compared to P25 and or their tiny percentage compared with P25.

Figure 1C presents the zeta potential values at different pH and shows the colloidal stability of the prepared nanocomposite in different media. At pH =7, the prepared nanocomposite possesses a net positive charge and relatively lower stability (zeta potential = +22.2 mV), while in acidic medium (pH = 2), it showed higher stability (zeta potential = + 48.6 mV). By contrast, in an alkaline medium (pH = 11), it possessed a net negative charge with a zeta potential of (-34.5 mV) corresponding to moderate stability [41]. Finally, at pH = 8.7, the net surface charge is zero, the point of zero charge (PZC).

Morphology and conjugation of P25 and rGO nanosheets was further revealed by SEM, TEM, and HR-TEM analyses as shown in **Figure 2A-C**. SEM and TEM analyses (high magnification) are presented in **Figure 1S**. SEM analysis **Figure 2A**, reveals the spherical morphology of P25 particles and the sheets of rGO constituting the nanocomposite. While the average particle size was found to be 22 nm from TEM analysis **Figure 2B**. Additionally, **Figure 2C** demonstrates HR-TEM analysis, confirming the conjugation between P25 and rGO sheets by revealing characteristic planes of both samples. Furthermore, **Figure 2S** presents STEM mapping analysis, confirming the distribution of Ag NPs on the P25 surface.

While **Figure 3S** shows the XRD, SEM, and TEM analyses of bare P25 sample, where the recorded peaks correspond to the rutile and Anatase phases of TiO_2 (JCPDS card number (21-1276) as previously explained. SEM confirmed the semi-spherical morphology of the particles which possess an average diameter of about 21 nm as revealed by the TEM analysis.

We also investigated the characterization of the rGO nanosheets used in our study. Our examination of the rGO nanosheets encompassed multiple facets. Firstly, Fourier-Transform Infrared (FTIR) analysis provided valuable insights into the molecular composition and bonding within the nanocomposite, contributing to our understanding of its intricate structure. Furthermore, SEM was used to confirm the unique surface characteristics of rGO (**Figure 4S)**.

316

317 **TNC supports MG63 proliferation.**

318 **Figure 3A** demonstrates that TNC at a concentration of 100 µg/ml significantly
319 increased the cell number of MG63 after 24 hours of incubation, with a remarkable
320 32% higher proliferation rate in TNC-treated cells compared to the control group ($p <$
321 0.0001). Furthermore, the combination of EB1089+FHBP+TNC showed a significantly
322 higher proliferation of MG63 after 3 days of culture compared to FHBP, EB1089, or
323 their combinations (**Figure 3B**). Notably, TNC addition to EB1089+FHBP resulted in
324 a remarkable 26.7% ± 3.8% higher proliferation rate ($p = 0.0001$), and the overall
325 combination of EB1089+FHBP+TNC exhibited an impressive 44.5% ± 1.6% higher
326 proliferation rate than the control group (**Figure 5S).**

327

328 **TNC promotes FHBP-induced MG63 maturation.**

329 Herein, we demonstrated that integration of rGO with the aforementioned combination
330 could significantly increase the ALP activity of MG63 (2-fold, $p < 0.0001$, **Figure 4A**).
331 This result was consistent with the morphological appearance of MG63 in the
332 EB1089+FHBP+TNC treatment group in which some cells exhibited a dendritic shape
333 (**Figure 4B**).

334

335 **MG63 maturation at polycatecholamine-functionalised TNC**
336 Comparing PDA and PNE coating capacity revealed a significantly higher potential of
337 PDA to entrap the FHBP over PNE (**Figure 6S**). As reported by Baldwin et al. [37], a
338 one-pot application of FHBP with dopamine hydrochloride afforded FHBP-PDA
339 coatings that supported MG63 maturation. Whilst we were able to generate similar
340 FHBP-PNE coatings these were not as effective in promoting EB1089-induced
341 differentiation. Consequently, work with PNE was halted. Tissue culture plastic was
342 co-functionalised with PDA, TNC and FHBP, the resultant complex promoted the
343 greatest extent of MG63 maturation, as supported by greater ALP activity, compared
344 to agents used in isolation (10-fold, $p < 0.0001$, **Figure 5A**). However, in comparison
345 to coated FHBP alone, there was significantly lower ALP activity (1.4-fold, $p < 0.0001$,

346 **Figure 5A**). These data suggest a reduction in FHBP adsorption following coating
347 suspension removal. To confirm the capacity of FHBP to bind to suspended TNC we
348 further investigated the binding capacity of both components.
349 It is also worth mentioning that seeding a high cell density (1.2 x 10^5) in
350 presence of the EB1089+FHBP combination with TNC promoted cell aggregation
351 (**Figure 5B**, first column from the right). This was further confirmed using alizarin red
352 staining as shown in **Figure 5C**.
353
354 **FHBP binds to TNC.**
355 To investigate the interaction between TNC and FHBP, TNC was incubated with FHBP
356 for one hour and then centrifuged to separate the TNC pellet from the suspended
357 FHBP (**Figure 6A**). The combination of the TNC pellet with EB1089 resulted in
358 significantly higher ALP activity compared to the supernatant+EB1089 group,
359 indicating a strong interaction between TNC and FHBP (**Figure 6B**).
360
361
362 **TNC improves osteoblast maturation through upregulation of OPN and OCN**
363 **gene expression.**
364 At the molecular level, after 3 days of culture, MG63 cells treated with the combined
365 formulation of EB1089, FHBP and TNC showed significant reduction in Collagen type
366 I (COL1A1) expression compared to the control group (2.5-fold change, $p < 0.0001$,
367 **Figure 7A**). Conversely, the combination of EB1089+FHBP+TNC exhibited
368 significantly higher expression of Osteopontin (OPN) mRNA compared to
369 EB1089+FHBP (2.3-fold, $p < 0.0001$, **Figure 7B**). Furthermore, Osteocalcin (OCN)
370 expression was 1.5-fold higher in the EB1089+FHBP+TNC group compared to
371 EB1089+FHBP ($p < 0.0001$) and 2.5-fold higher in the EB1089+FHBP group
372 compared to the control group ($p < 0.0001$, **Figure 7C**).
373
374 **Coating Ti-discs with TNC**
375 Coating Ti discs with a simple drop-casting technique at 60 °C/1.5 hrs and 37 °C/1hr
376 resulted in a lower contact angle of 51° ± 8.3° and 41.5° ± 8° respectively compared
377 to 56.7° ± 6.2° for blank, non-treated Ti discs (**Figure 8**). Furthermore, TNC-coated Ti
378 discs revealed no cytotoxic effect on MG63 seeded on the top of the discs as
379 confirmed by the MTS assay (**Figure 8**).

Discussion

Nanomaterials have revolutionized the field of bone tissue regeneration by offering unique properties and versatile applications. Among these nanomaterials, the P25/rGO/Ag nanocomposite discussed in this study holds great promise for enhancing bone regeneration. By combining the properties of P25, a titanium dioxide photocatalyst, and reduced graphene oxide (rGO), a two-dimensional carbon material, the nanocomposite exhibits synergistic effects that promote cell adhesion, proliferation, and controlled drug release. Understanding the composition, crystal structure, stability, and morphology of the P25/rGO/Ag nanocomposite is crucial for unlocking its full potential in bone tissue engineering, paving the way for the development of advanced biomaterials for effective bone regeneration.

The characterization and structural analysis of the P25/rGO/Ag nanocomposite revealed valuable insights into its composition and properties. X-ray diffraction (XRD) analysis showed characteristic peaks corresponding to specific crystallographic planes, confirming the presence of P25 and rGO. The observed peaks were in good agreement with the JCPDS card number of P25 [40], while the presence of rGO was confirmed by the detection of a characteristic carbon material peak. This analysis provided crucial information about the crystalline nature and phase composition of the nanocomposite. Furthermore, the XRD pattern indicated successful conjugation between P25 and rGO, as characteristic peaks of both materials were present. This suggests potential synergistic effects and enhanced properties in the nanocomposite.

Zeta potential measurements provided insights into the colloidal stability of the prepared nanocomposite at different pH values. The nanocomposite exhibited a net positive charge at pH 7, indicating lower stability, while it showed higher stability in an acidic medium (pH 2) and a net negative charge with moderate stability in an alkaline medium (pH 11) [41]. The point of zero charge (PZC) was determined to be at pH 8.7, where the net surface charge is zero. This information is crucial for understanding the behavior and stability of the nanocomposite under different environmental conditions. Additionally, morphology analysis using SEM, TEM, and HR-TEM techniques provided visual evidence of the spherical morphology of P25 particles and the presence of rGO

412 sheets in the nanocomposite. These analyses further confirmed the conjugation
413 between P25 and rGO nanosheets, as characteristic planes of both materials were
414 observed.

415 In order to explore the potential of TNC in bone regeneration, we conducted
416 investigations using MG63 cell lines. Our findings reveal that TNC exhibits a
417 remarkable ability to promote the proliferation of MG63 cells. This increase in the
418 proliferation aligns with our previous results [11, 12] which confirms that TNC is
419 noncytotoxic and biocompatible. This increase in cell proliferation can be attributed to
420 the rough surface area of graphene which provides a large surface area for the cells
421 to proliferate. The surface feature of the rGO has been investigated in our pervious
422 publication in which we have reported that graphene flakes agglomerate into a high
423 surface area as confirmed by scanning electron microscopy (SEM) [12].

424 In addition to the surface area effect, nanoparticles have been found to act as
425 signaling mediators or modulators, influencing cellular signaling pathways that
426 regulate both proliferation and differentiation. For instance, studies have shown that
427 Graphene Oxide Quantum Dots nanoparticles can activate the Wnt/β-catenin pathway
428 in bone marrow-derived mesenchymal stem cells (BMSCs), resulting in increased
429 proliferation and enhanced osteogenic differentiation [42]. Similarly, gold
430 nanoparticles (AuNPs) have been reported to enhance the proliferation of human
431 periodontal ligament stem cells (hPDLSC) through the activation of the Wnt/β-catenin
432 signaling pathway [43].

433 It is also noteworthy that we observed a significant increase in cell number of
434 MG63 cells after 24 hours in the presence of TNC. However, at the 3-day time point,
435 there was no significant difference in cell proliferation between the TNC alone group
436 and the control group without TNC.

437 One possible explanation for this observation is the initial stimulation of cell
438 growth induced by TNC, leading to an initial surge in cell number. However, over the
439 subsequent 48 hours, the cells in the control group may have caught up in terms of
440 proliferation, resulting in a comparable cell number between the two groups. This
441 suggests that the proliferative effects of TNC may be transient or time-dependent.

442 We have demonstrated in our lab that FHBP in combination with 1,25D initiates
443 osteoblast maturation as confirmed by a dramatic increase in ALP activity [2].
444 Similarly, the findings of this study provide evidence that the integration of TNC with
445 the combination of FHBP and the 1,25D analogue, EB1089, significantly enhances
446 ALP activity in MG63 cells. The observed 2-fold increase in ALP activity suggests an
447 enhancement in osteoblast maturation and functionality, which is crucial for bone
448 regeneration processes.

449 Furthermore, the morphological appearance of MG63 cells in the
450 EB1089+FHBP+TNC treatment group supports the notion of osteoblast maturation.
451 The presence of dendritic-shaped cells indicates the transition from osteoblasts to
452 mature osteocytes, which are key cells involved in bone remodeling and maintenance.
453 As described by Dallas and Bonewald [44], this characteristic shape represents the
454 cell transition from osteoblast to mature osteocyte. This result was consistent with that
455 reported by Filova et al. who demonstrated that culturing MG63 on nanosized
456 hydroxyapatite enhanced their differentiation and exhibited similar morphology and
457 this was further confirmed by an increase in OPN expression [45].

458 We have explored the use of PDA reactive platforms to capture agents at the
459 Ti surface that are known to target bone-forming osteoblasts [37]. The use of PDA as
460 a reactive film for many materials has emerged from our understanding of how edible
461 marine mussels (Mytilus edulis) tenaciously attach to wet surfaces. Specialized
462 mussel foot proteins are rich in lysine and DOPA residues, each of which bears amino
463 and catechol groups respectively, and which are responsible for the adhesive
464 properties. Interestingly if dopamine hydrochloride is dissolved in mildly alkaline (~pH
465 8) solutions it spontaneously polymerizes to PDA. Any object that is present during
466 polymerization becomes functionalized with a PDA thin film, even Teflon! The PDA in
467 turn is reactive toward a multitude of agents including peptides, proteins, lipids,
468 oligonucleotides, and noble metals. The reactive nature of PDA enables further
469 material functionalization to suit a particular application, e.g., affinity sorbents and
470 catalytic platforms [46].

471 The observed formation of cell aggregates at a high cell density in the presence
472 of the combination of EB1089+FHBP with TNC (**Figure 5C**) is noteworthy. Similar
473 aggregates have been reported when culturing MG63 on vitamin D3-entrapped
474 calcium phosphate films [47]. These aggregates indicate the potential of the
475 combination treatment to promote the aggregation of cells and the formation of nodular

476 structures, which are characteristic of osteoblast maturation and bone tissue
477 development.

478 Previous studies have demonstrated that there is an electrostatic interaction
479 between GO and the acyl chain of phospholipid membranes [48-50]. Of further
480 significance is the recent finding that LPA adsorbs strongly to graphene through
481 hydrogen bonding [51]. In addition, it is widely recognised that phosphonic acids, of
482 which LPA and FHBP belong, bind strongly to TiO_2 [52] and we have previously
483 reported that FHBP can readily functionalise Ti [3]. Hence, we hypothesized that our
484 P25/rGO/Ag composite may interact with FHBP. The results of our experiment
485 support this hypothesis, as the combination of TNC and FHBP demonstrated
486 significantly higher ALP activity compared to the group treated with the FHBP-depleted
487 supernatant+EB1089. This suggests a facile and robust interaction between TNC and
488 FHBP, highlighting the potential for TNC to effectively interact with and carry FHBP,
489 potentially enhancing its functionality in bone regeneration applications.

490 COL1A1 is a major component of the bone matrix that is synthesized by
491 osteoblasts [53]. The expression of COL1A1 varies during the differentiation of
492 osteoblasts into mature osteocytes and is typically highest in immature osteoblasts
493 and lowest in mature osteocytes. The higher expression of COL1A1 in the treatment
494 groups indicates the potential of TNC, EB1089, and FHBP to promote osteogenic
495 differentiation. OPN is a well-defined marker expressed in the late stage of osteogenic
496 differentiation. The higher expression of OPN here aligned with the higher ALP activity
497 which supports the potential of TNC to promote osteogenic differentiation [54, 55].
498 OCN was also reported as an essential modulator of the mineral species maturation
499 during osteogenic differentiation [56]. The higher expression of OCN in the treatment
500 groups further supports the enhanced osteoblast maturation induced by the
501 combination of EB1089, FHBP, and TNC.

502 From our experience, we have demonstrated that OPN expression significantly
503 increases in BMSCs through the P38 pathway. This increase was correlated to
504 significantly higher osteogenic differentiation and mineralization in BMSCs compared
505 to the low osteogenic potential expressed by adipose derived stem cells (ASCs) as
506 confirmed by Alizarin red.

507 A recent study investigating the genetic profiling of MSCs cultured on graphene
508 sheds light on the osteogenic signaling pathways affected by this material [57]. The
509 findings suggest that graphene plays a crucial role in promoting osteogenic

510 differentiation in BMSCs by activating key signaling pathways. The observed
511 upregulation of ALP, BMP, SMAD3, TGFB, and OPN indicates the involvement of
512 BMP and TGF-β signalling in the differentiation of osteoblasts. Moreover, when
513 comparing BMSCs cultured on graphene to ASCs, the study reveals significant
514 upregulation of transcription factors DLX5, RUNX2, SOX9, and SP7, implying that
515 graphene preferentially induces the commitment of BMSCs towards the osteogenic
516 lineage.

517 Herein this study, the combination of EB1089+FHBP promotes MG63
518 maturation. Furthermore, the addition of TNC to this combination resulted in a more
519 advanced stage of maturation, as evidenced by the higher expression of osteogenic
520 markers such as OPN and OCN (**Figure 7D**). Taken together, the TNC-FHBP complex
521 supported greater EB1089-induced maturation, this may be attributed to the surface
522 area of TNC, future studies of which will explore this possibility.

523 Herein, we have demonstrated that coating Ti discs with TNC using the drop-
524 casting technique effectively enhances the hydrophilic nature of the Ti surface. This
525 improved hydrophilicity is beneficial for promoting cell adhesion and interaction with
526 the coated Ti discs. Kang et al. [56] also reported similar results, in which the rGO
527 resulted in a water contact angle of roughly 76° compared to 127° for blank Ti,
528 supporting the notion that the presence of graphene-based materials, such as TNC,
529 can enhance the hydrophilicity of Ti surfaces [58].

530 The observed variations in contact angle between Ti discs coated with TNC at
531 different temperatures can be understood within the context of wettability-regulated
532 phenomena and surface thermodynamics. Contact angle measurements serve as a
533 valuable tool for quantifying macroscopic surface wettability and are particularly
534 relevant for understanding heat transfer processes like boiling [59]. The temperature
535 dependence of contact angles has been extensively investigated, revealing distinct
536 trends in different temperature regimes [59]. In the case of our study, coating Ti discs
537 with TNC at 37°C/1 hr and 60°C/1.5 hrs resulted in varying contact angles. At 37°C,
538 the coating process may facilitate slower molecular adsorption and self-assembly of
539 TNC molecules on the surface. This moderate temperature could potentially lead to a
540 more organized arrangement of molecules and stronger interactions with the Ti disc
541 surface, resulting in a lower contact angle. On the other hand, at 60°C, the faster
542 deposition process might hinder extensive molecular rearrangement, potentially
543 leading to a less ordered TNC layer and, consequently, a higher contact angle [60].

The interplay between temperature, coating time, and molecular arrangement during the coating process contributes to the observed contact angle variations. These findings align with the trends seen in other studies investigating surface modification and wettability effects [60].

Furthermore, the cytotoxicity assessment using the MTS-PMS assay confirmed that TNC-coated Ti discs did not exhibit any toxic effects on MG63 cells. This finding is consistent with the earlier data presented and aligns with the findings reported by Kang et al. [58]. The non-cytotoxic nature of TNC-coated Ti discs suggests their biocompatibility and suitability for use in biomedical applications, particularly in promoting cell adhesion and proliferation.

Limitations and Future Directions

While the present study offers valuable insights into the osteogenic potential of TNC nanocomposite, there are some experimental aspects that were not addressed within the scope of this research. The absence of antibacterial activity testing is considered as a limitation of this study, and its inclusion in future research could provide valuable insights into the broader efficacy of TNC for various applications.

Conclusion

The integration of P25/rGO/Ag nanocomposite potentiates FHBP-induced osteoblast maturation as supported by increased OPN and OCN mRNA and total ALP activity. The nanocomposite under investigation offers a platform for osteoblast maturation and osteointegration and is proposed for robust bone regeneration. Further studies are required to investigate coating bone biomaterials, especially Ti with a P25/rGO/Ag nanocomposite.

Summary points

- A ternary nanocomposite (TNC) consisting of P25/rGO/Ag shows biocompatibility with MG63 osteoblast-like cells.
- TNC does not exhibit cytotoxic effects on MG63 cells, indicating its potential safety for cellular applications.

576 • The inclusion of TNC in the co-treatment of MG63 cells with EB1089 and FHBP
577 enhances osteoblast maturation.
578 • TNC treatment leads to increased alkaline phosphatase (ALP) activity, which is
579 indicative of enhanced osteoblast maturation.
580 • The expression of osteopontin (OPN) and osteocalcin (OCN) genes is
581 upregulated in MG63 cells treated with EB1089-FHBP-TNC, suggesting
582 increased osteogenic potential.
583 • The integration of a P25/rGO/Ag nanocomposite enhances FHBP-induced
584 osteoblast maturation, as evidenced by increased OPN and OCN mRNA
585 expression.
586 • TNC serves as a promising carrier for FHBP, highlighting its potential
587 application in bone regenerative settings.
588 • The nanocomposite provides a platform for osteoblast maturation and
589 osteointegration, suggesting its potential for robust bone regeneration.
590 • The study emphasizes the importance of TNC in promoting osteogenic
591 differentiation and suggests its potential use in improving bone healing and
592 regenerative therapies.
593 • Further investigations are needed to explore the coating of bone biomaterials,
594 particularly titanium, with the P25/rGO/Ag nanocomposite.
595

596 **References**

597

598 1. Eichholtz T, Jalink K, Fahrenfort I, Moolenaar WH. The bioactive phospholipid lysophosphatidic
599 acid is released from activated platelets. *Biochem J* 291 (Pt 3)(Pt 3), 677-680 (1993).
600 2. Mansell JP, Nowghani M, Pabbruwe M, Paterson I, Smith A, Blom A. Lysophosphatidic acid and
601 calcitriol co-operate to promote human osteoblastogenesis: requirement of albumin-bound
602 LPA. *Prostaglandins & other lipid mediators* 95(1-4), 45-52 (2011).
603 3. Shiel AI, Ayre WN, Blom AW *et al*. Development of a facile fluorophosphonate-functionalised
604 titanium surface for potential orthopaedic applications. *Journal of Orthopaedic Translation* 23
605 140-151 (2020).
606 4. Mansell JP, Cooke M, Read M *et al*. Chitinase 3-like 1 expression by human (MG63) osteoblasts
607 in response to lysophosphatidic acid and 1,25-dihydroxyvitamin D3. *Biochimie* 128-129 193-
608 200 (2016).
609 5. Elkhenany H, Elkodous MA, Newby SD, El-Derby AM, Dhar M, El-Badri N. Tissue engineering
610 modalities and nanotechnology. In: *Regenerative medicine and stem cell biology*,
611 (Ed.^(Eds).Springer 289-322 (2020).
612 6. El-Badri N, Elkhenany H. Toward the nanoengineering of mature, well-patterned and
613 vascularized organoids. *Nanomedicine* 16(15), 1255-1258 (2021).

614 7. Strub M, Van Bellinghen X, Fioretti F *et al*. Maxillary Bone Regeneration Based on
615 Nanoreservoirs Functionalized ε-Polycaprolactone Biomembranes in a Mouse Model of Jaw
616 Bone Lesion. *Biomed Res Int* 2018 7380389 (2018).
617 8. Elkhateeb OM, Badawy MEI, Noreldin AE, Abou-Ahmed HM, El-Kammar MH, Elkhenany HA.
618 Comparative evaluation of propolis nanostructured lipid carriers and its crude extract for
619 antioxidants, antimicrobial activity, and skin regeneration potential. *BMC Complementary*
620 *Medicine and Therapies* 22(1), 256 (2022).
621 9. Bonilla P, Hernandez J, Giraldo E *et al*. Human-Induced Neural and Mesenchymal Stem Cell
622 Therapy Combined with a Curcumin Nanoconjugate as a Spinal Cord Injury Treatment.
623 *International Journal of Molecular Sciences* 22(11), 5966 (2021).
624 10. Elkhenany H, Bonilla P, Giraldo E *et al*. A Hyaluronic Acid Demilune Scaffold and Polypyrrole-
625 Coated Fibers Carrying Embedded Human Neural Precursor Cells and Curcumin for Surface
626 Capping of Spinal Cord Injuries. *Biomedicines* 9(12), 1928 (2021).
627 11. Elkhenany H, Amelse L, Lafont A *et al*. Graphene supports in vitro proliferation and osteogenic
628 differentiation of goat adult mesenchymal stem cells: potential for bone tissue engineering.
629 *Journal of Applied Toxicology* 35(4), 367-374 (2015).
630 12. Elkhenany H, Bourdo S, Hecht S *et al*. Graphene nanoparticles as osteoinductive and
631 osteoconductive platform for stem cell and bone regeneration. *Nanomedicine:*
632 *Nanotechnology, Biology and Medicine* 13(7), 2117-2126 (2017).
633 13. Malhotra R, Han Y, Nijhuis CA, Silikas N, Castro Neto AH, Rosa V. Graphene nanocoating
634 provides superb long-lasting corrosion protection to titanium alloy. *Dental Materials*
635 doi:https://doi.org/10.1016/j.dental.2021.08.004 (2021).
636 14. Du H, Zhu X, Fan C, Xu S, Wang Y, Zhou Y. Oxidative damage and OGG1 expression induced by
637 a combined effect of titanium dioxide nanoparticles and lead acetate in human hepatocytes.
638 *Environ Toxicol* 27(10), 590-597 (2012).
639 15. Saquib Q, Al-Khedhairy AA, Siddiqui MA, Abou-Tarboush FM, Azam A, Musarrat J. Titanium
640 dioxide nanoparticles induced cytotoxicity, oxidative stress and DNA damage in human
641 amnion epithelial (WISH) cells. *Toxicol In Vitro* 26(2), 351-361 (2012).
642 16. Hong F, Wu N, Zhao X *et al*. Titanium dioxide nanoparticle-induced dysfunction of cardiac
643 hemodynamics is involved in cardiac inflammation in mice. *J Biomed Mater Res A* 104(12),
644 2917-2927 (2016).
645 17. Eldebany N, Abd Elkodous M, Tohamy H *et al*. Gelatin loaded titanium dioxide and silver oxide
646 nanoparticles: implication for skin tissue regeneration. *Biological Trace Element Research*
647 199(10), 3688-3699 (2021).
648 18. Nikpasand A, Parvizi MR. Evaluation of the Effect of Titatnium Dioxide Nanoparticles/Gelatin
649 Composite on Infected Skin Wound Healing; An Animal Model Study. *Bull Emerg Trauma* 7(4),
650 366-372 (2019).
651 19. Kubota S, Johkura K, Asanuma K *et al*. Titanium oxide nanotubes for bone regeneration. *J*
652 *Mater Sci Mater Med* 15(9), 1031-1035 (2004).
653 20. Souza W, Piperni SG, Laviola P *et al*. The two faces of titanium dioxide nanoparticles bio-
654 camouflage in 3D bone spheroids. *Sci Rep* 9(1), 9309 (2019).
655 21. Niska K, Pyszka K, Tukaj C, Wozniak M, Radomski MW, Inkielewicz-Stepniak I. Titanium dioxide
656 nanoparticles enhance production of superoxide anion and alter the antioxidant system in
657 human osteoblast cells. *Int J Nanomedicine* 10 1095-1107 (2015).
658 22. Zhang Y, Yu W, Jiang X, Lv K, Sun S, Zhang F. Analysis of the cytotoxicity of differentially sized
659 titanium dioxide nanoparticles in murine MC3T3-E1 preosteoblasts. *J Mater Sci Mater Med*
660 22(8), 1933-1945 (2011).
661 23. Quinn J, Mcfadden R, Chan C-W, Carson L. Titanium for Orthopedic Applications: An Overview
662 of Surface Modification to Improve Biocompatibility and Prevent Bacterial Biofilm Formation.
663 *iScience* 23(11), 101745 (2020).

24. Geetha M, Singh AK, Asokamani R, Gogia AK. Ti based biomaterials, the ultimate choice for orthopaedic implants–a review. *Progress in materials science* 54(3), 397-425 (2009).
25. Nie BE, Huo S, Qu X *et al*. Bone infection site targeting nanoparticle-antibiotics delivery vehicle to enhance treatment efficacy of orthopedic implant related infection. *Bioactive Materials* 16 134-148 (2022).
26. Qing Y, Cheng L, Li R *et al*. Potential antibacterial mechanism of silver nanoparticles and the optimization of orthopedic implants by advanced modification technologies. *Int J Nanomedicine* 13 3311-3327 (2018).
27. Khalandi B, Asadi N, Milani M *et al*. A Review on Potential Role of Silver Nanoparticles and Possible Mechanisms of their Actions on Bacteria. *Drug Res (Stuttg)* 67(2), 70-76 (2017).
28. Klueh U, Wagner V, Kelly S, Johnson A, Bryers JD. Efficacy of silver-coated fabric to prevent bacterial colonization and subsequent device-based biofilm formation. *J Biomed Mater Res* 53(6), 621-631 (2000).
29. Long YM, Hu LG, Yan XT *et al*. Surface ligand controls silver ion release of nanosilver and its antibacterial activity against Escherichia coli. *Int J Nanomedicine* 12 3193-3206 (2017).
30. Gon S, Faulkner MJ, Beckwith J. In vivo requirement for glutaredoxins and thioredoxins in the reduction of the ribonucleotide reductases of Escherichia coli. *Antioxid Redox Signal* 8(5-6), 735-742 (2006).
31. Roy S, Martel J, Tenenhouse HS. Comparative effects of 1, 25-dihydroxyvitamin D3 and EB 1089 on mouse renal and intestinal 25-hydroxyvitamin D3-24-hydroxylase. *Journal of Bone and Mineral Research* 10(12), 1951-1959 (1995).
32. Carlberg C, Mathiasen IS, Saurat J-H, Binderup L. The 1, 25-dihydroxyvitamin D3 (VD) analogues MC903, EB1089 and KH1060 activate the VD receptor: homodimers show higher ligand sensitivity than heterodimers with retinoid X receptors. *The Journal of steroid biochemistry and molecular biology* 51(3-4), 137-142 (1994).
33. Binderup L, Carlberg C, Kissmeyer A, Latini S, Mathiasen I, Hansen CM. The need for new vitamin D analogues: mechanisms of action and clinical applications. 55-63 (1994).
34. Staudenmaier L. Verfahren zur darstellung der graphitsäure. *Berichte der deutschen chemischen Gesellschaft* 31(2), 1481-1487 (1898).
35. Abd Elkodous M, S. El-Sayyad G, Abdel Maksoud MIA *et al*. Nanocomposite matrix conjugated with carbon nanomaterials for photocatalytic wastewater treatment. *Journal of Hazardous Materials* 410 124657 (2021).
36. Abd Elkodous M, El-Sayyad GS, Youssry SM *et al*. Carbon-dot-loaded CoxNi1−xFe2O4; x = 0.9/SiO2/TiO2 nanocomposite with enhanced photocatalytic and antimicrobial potential: An engineered nanocomposite for wastewater treatment. *Scientific Reports* 10(1), 11534 (2020).
37. Baldwin F, Craig TJ, Shiel AI, Cox T, Lee K, Mansell JP. Polydopamine-lysophosphatidate-functionalised titanium: A novel hybrid surface finish for bone regenerative applications. *Molecules* 25(7), 1583 (2020).
38. Neary G, Blom AW, Shiel AI, Wheway G, Mansell JP. Development and biological evaluation of fluorophosphonate-modified hydroxyapatite for orthopaedic applications. *Journal of Materials Science: Materials in Medicine* 29(8), 1-10 (2018).
39. Lancaster ST, Blackburn J, Blom A, Makishima M, Ishizawa M, Mansell JP. 24, 25-Dihydroxyvitamin D3 cooperates with a stable, fluoromethylene LPA receptor agonist to secure human (MG63) osteoblast maturation. *Steroids* 83 52-61 (2014).
40. Hou J, Lan X, Shi J *et al*. A mild and simple method to fabricate commercial TiO2 (P25) and C60 composite for highly enhancing H2 generation. *International Journal of Hydrogen Energy* 45(4), 2852-2861 (2020).
41. Abd Elkodous M, El-Sayyad GS, Mohamed AE *et al*. Layer-by-layer preparation and characterization of recyclable nanocomposite (Co x Ni 1− x Fe 2 O 4; X= 0.9/SiO 2/TiO 2). *Journal of Materials Science: Materials in Electronics* 30(9), 8312-8328 (2019).

42. Xu D, Wang C, Wu J *et al*. Effects of Low-Concentration Graphene Oxide Quantum Dots on Improving the Proliferation and Differentiation Ability of Bone Marrow Mesenchymal Stem Cells through the Wnt/β-Catenin Signaling Pathway. *ACS Omega* 7(16), 13546-13556 (2022).
43. Li C, Li Z, Zhang Y, Fathy AH, Zhou M. The role of the Wnt/β-catenin signaling pathway in the proliferation of gold nanoparticle-treated human periodontal ligament stem cells. *Stem cell research & therapy* 9(1), 1-10 (2018).
44. Dallas SL, Bonewald LF. Dynamics of the transition from osteoblast to osteocyte. *Annals of the New York Academy of Sciences* 1192(1), 437-443 (2010).
45. Filova E, Suchý T, Sucharda Z *et al*. Support for the initial attachment, growth and differentiation of MG-63 cells: a comparison between nano-size hydroxyapatite and micro-size hydroxyapatite in composites. *International journal of nanomedicine* 9 3687 (2014).
46. Ryu JH, Messersmith PB, Lee H. Polydopamine Surface Chemistry: A Decade of Discovery. *ACS Applied Materials & Interfaces* 10(9), 7523-7540 (2018).
47. Choi YS, Hong YJ, Hur J *et al*. Bone nodule formation of Mg63 cells is increased by the interplay of signaling pathways cultured on vitamin D3-entrapped calcium phosphate films. *Animal cells and systems* 13(4), 363-370 (2009).
48. Frost R, Jönsson GE, Chakarov D, Svedhem S, Kasemo B. Graphene Oxide and Lipid Membranes: Interactions and Nanocomposite Structures. *Nano Letters* 12(7), 3356-3362 (2012).
49. Chen J, Zhou G, Chen L, Wang Y, Wang X, Zeng S. Interaction of Graphene and its Oxide with Lipid Membrane: A Molecular Dynamics Simulation Study. *The Journal of Physical Chemistry C* 120(11), 6225-6231 (2016).
50. Tsuzuki K, Okamoto Y, Iwasa S, Ishikawa R, Sandhu A, Tero R. Reduced Graphene Oxide as the Support for Lipid Bilayer Membrane. *Journal of Physics: Conference Series* 352(1), 012016 (2012).
51. Liu W, Luo H, Wei Q *et al*. Electrochemically derived nanographene oxide activates endothelial tip cells and promotes angiogenesis by binding endogenous lysophosphatidic acid. *Bioactive Materials* 9 92-104 (2022).
52. Queffelec C, Petit M, Janvier P, Knight DA, Bujoli B. Surface modification using phosphonic acids and esters. *Chemical reviews* 112(7), 3777-3807 (2012).
53. Blair HC, Larrouture QC, Li Y *et al*. Osteoblast Differentiation and Bone Matrix Formation In Vivo and In Vitro. *Tissue Eng Part B Rev* 23(3), 268-280 (2017).
54. Elkhenany H, Amelse L, Caldwell M, Abdelwahed R, Dhar M. Impact of the source and serial passaging of goat mesenchymal stem cells on osteogenic differentiation potential: implications for bone tissue engineering. *Journal of animal science and biotechnology* 7(1), 1-13 (2016).
55. Luu HH, Song WX, Luo X *et al*. Distinct roles of bone morphogenetic proteins in osteogenic differentiation of mesenchymal stem cells. *Journal of Orthopaedic research* 25(5), 665-677 (2007).
56. Tsao YT, Huang YJ, Wu HH, Liu YA, Liu YS, Lee OK. Osteocalcin Mediates Biomineralization during Osteogenic Maturation in Human Mesenchymal Stromal Cells. *Int J Mol Sci* 18(1), (2017).
57. Macdonald AF, Trotter RD, Griffin CD *et al*. Genetic profiling of human bone marrow and adipose tissue-derived mesenchymal stem cells reveals differences in osteogenic signaling mediated by graphene. *Journal of nanobiotechnology* 19 1-18 (2021).
58. Kang MS, Jeong SJ, Lee SH *et al*. Reduced graphene oxide coating enhances osteogenic differentiation of human mesenchymal stem cells on Ti surfaces. *Biomaterials Research* 25(1), 1-9 (2021).
59. Song J-W, Fan L-W. Temperature dependence of the contact angle of water: A review of research progress, theoretical understanding, and implications for boiling heat transfer. *Advances in Colloid and Interface Science* 288 102339 (2021).

60. Strnad G, Chirila N, Petrovan C, Russu O. Contact Angle Measurement on Medical Implant Titanium Based Biomaterials. *Procedia Technology* 22 946-953 (2016).

Reference Annotation

(**) M. S. Kang et al., "Reduced graphene oxide coating enhances osteogenic differentiation of human mesenchymal stem cells on Ti surfaces," Biomaterials Research, vol. 25, no. 1, pp. 1-9, 2021.

(The authors have investigated the effect of reduced graphene on the osteogenic differentiation of stem cells, which is relevant to our study as we are exploring the enhanced maturation of MG63 cells using TNC as a carrier)

(**) H. Elkhenany et al., "Graphene nanoparticles as osteoinductive and osteoconductive platform for stem cell and bone regeneration," Nanomedicine: Nanotechnology, Biology and Medicine, vol. 13, no. 7, pp. 2117-2126, 2017/10/01/ 2017, doi: http://dx.doi.org/10.1016/j.nano.2017.05.009.

(This reference is interesting as it investigates the effect of reduced graphene nanoparticles at in vitro and in vivo studies, supporting its potential to enhance bone regeneration. This aligns with our research on TNC as a promising carrier for FHBP in a bone regenerative setting.)

(**) S. T. Lancaster, J. Blackburn, A. Blom, M. Makishima, M. Ishizawa, and J. P. Mansell, "24, 25-Dihydroxyvitamin D3 cooperates with a stable, fluoromethylene LPA receptor agonist to secure human (MG63) osteoblast maturation," Steroids, vol. 83, pp. 52-61, 2014.

(This reference is interesting as it investigates the integrative potential of Vitamin D3 and LPA in promoting osteoblast maturation. Understanding the cooperative effects of different molecules on cell maturation can provide insights relevant to our study.)

(*) S. L. Dallas and L. F. Bonewald, "Dynamics of the transition from osteoblast to osteocyte," Annals of the New York Academy of Sciences, vol. 1192, no. 1, pp. 437-443, 2010.

(This reference is interesting as it clarifies the molecular basis of osteoblast maturation and transition to osteocyte. The information provided can help contextualize our study's focus on enhancing the maturation of MG63 cells.)

Figure legends

Figure 1. XRD analysis of (A) TNC (P25/rGO/Ag nanocomposite), (B) rGO nanosheets and (C) Zeta potential at different pH of TNC.

Figure 2. (A) SEM analysis (B) TEM analysis, and (C) HR-TEM analysis of TNC (P25/rGO/Ag) nanocomposite.

Figure 3. Biocompatibility of TNC. (A) MG63 viability and cell growth in presence of TNC after 24 hrs. (B) MTS/PMS assay of MG63 after 3 days of culture with EB1089, FHBP, and TNC. Data are represented as the mean ± SD (*$p < 0.05$, ***$p < 0.001$ and ****$p < 0.0001$).

Figure 4. TNC enhance MG63 maturation in presence of EB1089 and FHBP. (A) Quantitative analysis of ALP activity, data are represented as the mean ± SD (****$p < 0.0001$). (B) Morphological changes of MG63 in EB1089+FHBP+TNC group showing osteocyte-like cells with characteristic dendrites morphology as described by Blank and Sims 2019, 20x image, the cells were highlighted with blue colour.

Figure 5. Coating polystyrene plate with catecholamines. (A) Assessment of TNC inclusion to EB1089+FHBP combination on MG63 maturation using ALP assay. Data are represented as the mean ± SD (**$p < 0.01$, and ****$p < 0.0001$). (B) Representative images showing the morphological appearance of MG63 seeded at density of 120k on surfaces coated with EB1089, FHBP, TNC or combination of 2 or more of them with the aid of PDA. Also, uncoated groups treated with EB1089+FHBP with and without TNC were imaged. (C) Alizarin red staining of MG63 (1.2×10^5 cells/mL/well) suspended in EB1089+FHBP+TNC showing cell aggregation after 3 days of culture in an uncoated regular well plate.

Figure 6. Evidence for the binding of FHBP to TNC after stirring for 1 hour at 25 °C. (A) Schematic diagram showing the experiment design. Created with BioRender.com. (B) Quantitative analysis of ALP activity of MG63 in the presence of supernatant and TNC pellet with and without EB1089. Groups treated with EB1089, FHBP, EB1089+FHBP, EB1089+FHBP+TNC as well as non-treated cells were included for better comparative evaluation. Data are represented as the mean ± SD (****$p < 0.0001$).

Figure 7. Quantitative real-time polymerase chain reaction analysis. The expression levels of mRNAs (A) collagen I (Col1), (B) osteopontin (OPN) and (C) osteocalcin (OCN) normalized to GAPDH in MG63 non-treated as control and treated with EB1089, FHBP, TNC and their combinations as determined by real-time qRT-PCR. The data are represented as the mean ± SD (****$p < 0.0001$). (D) Schematic diagram showing cell maturation status based on mRNA expression as well as ALP analysis. Graph was created with BioRender.com.

Figure 8. Surface contact angle measurements of blank-Ti. (A) and TNC-Ti discs coated by drop casting at 60 °C (B) and 37 °C (C). (D) MTS/PMS assay of MG63 after 3 days of culture on the top of blank-Ti, TNC-Ti 60 °C and TNC-Ti 37 °C. Data are represented as the mean ± SD (*$p < 0.05$).

Supplementary Materials:

Figure 1S. a) SEM analysis (high magnification) of the prepared nanocomposite and b) TEM analysis.

Figure 2S. a) TEM analysis, b) STEM mapping analysis showing the distribution of Ti, c) Ag, and d) Ag overlap on Ti surface.

Figure 3S. P25 characterization. (A) XRD analysis, (B) SEM analysis and (C) TEM analysis.

Figure 4S. FTIR analysis of the prepared nanocomposite, b) SEM analysis of employed rGO, c) magnified SEM image of rGO sample.

Figure 5S. Proliferation rate (%) of MG63 at day 3. The proliferation rates were normalized to the control group.

Figure 6S. Coating polystyrene plate with catecholamines. Assessment of catecholamines PNE and PDA for FHBP coating efficacy using ALP assay.

Figure 1S

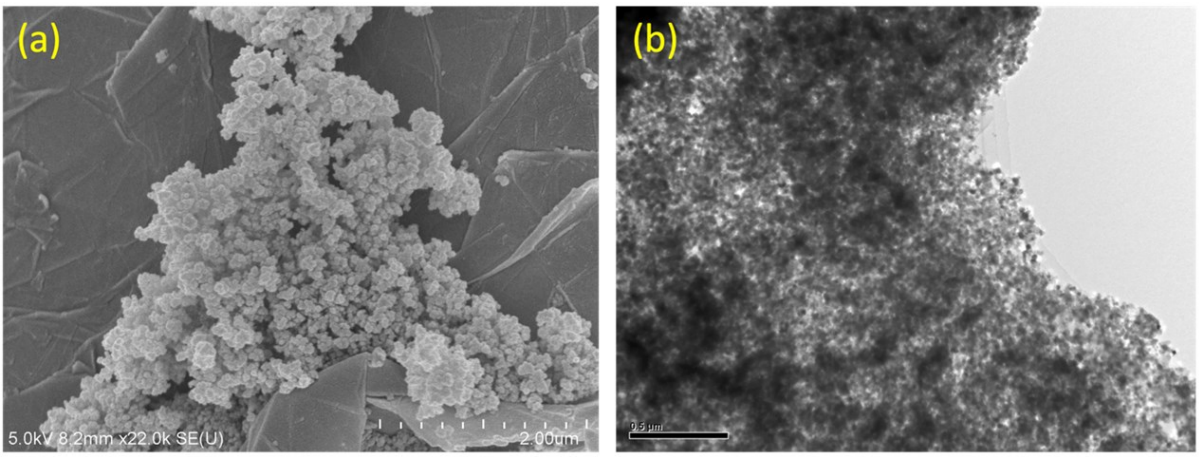

870 **Figure 2S**

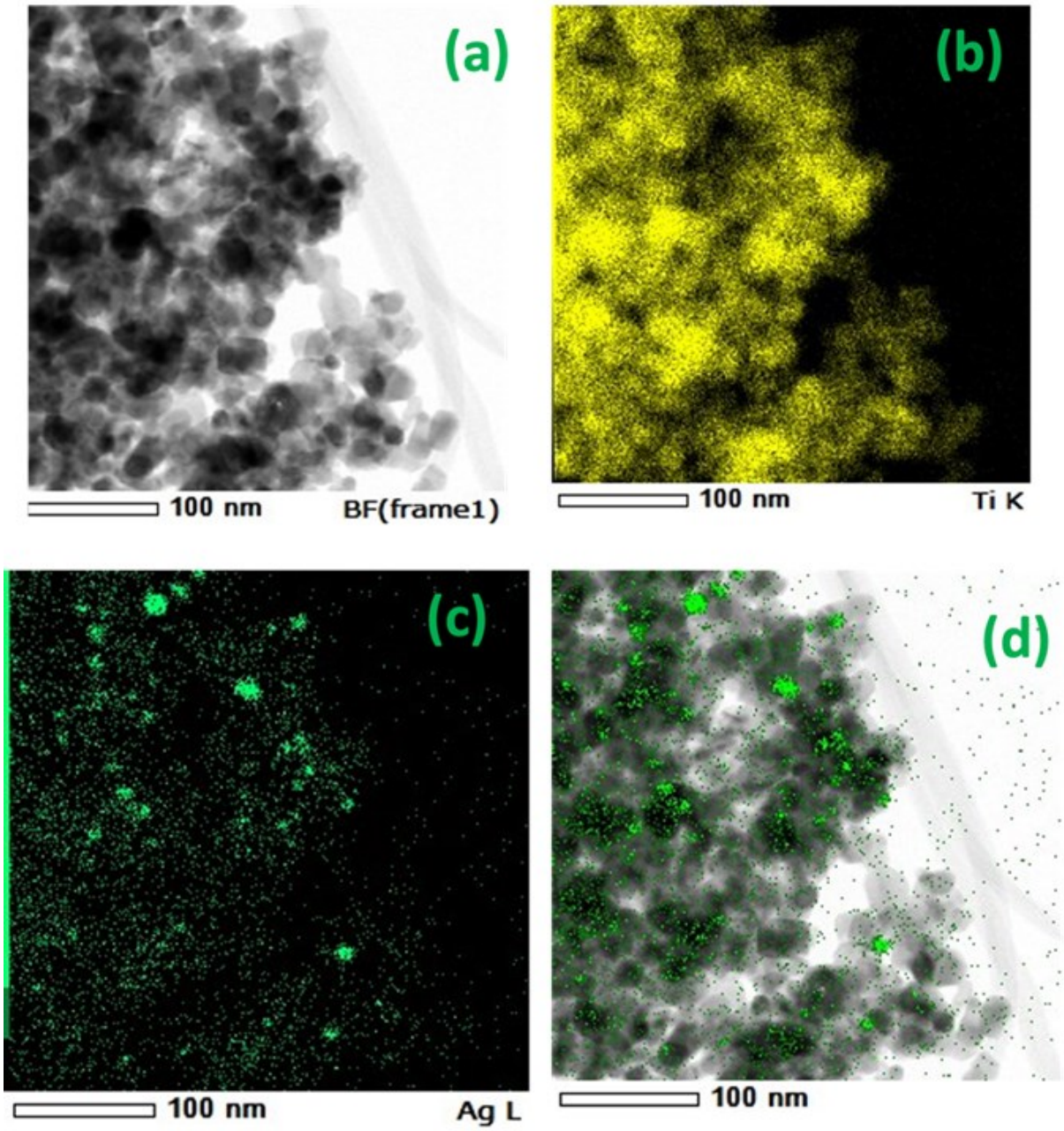

871

872

873

874

875

876

877

878

879

Figure 3S

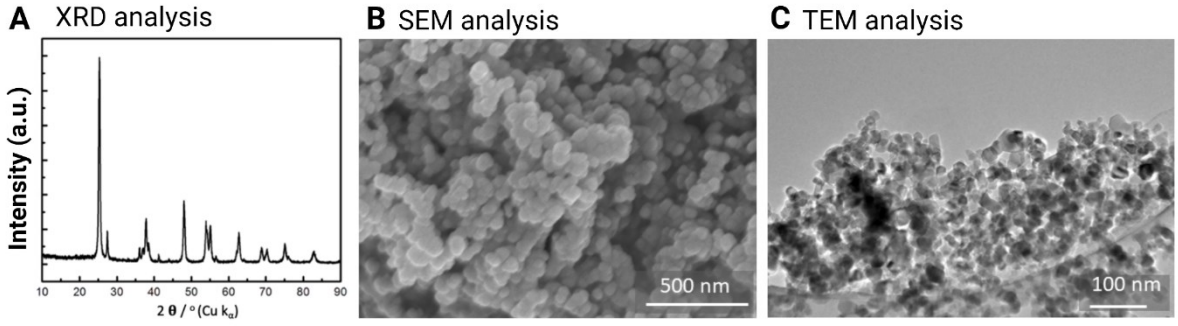

Figure 4S

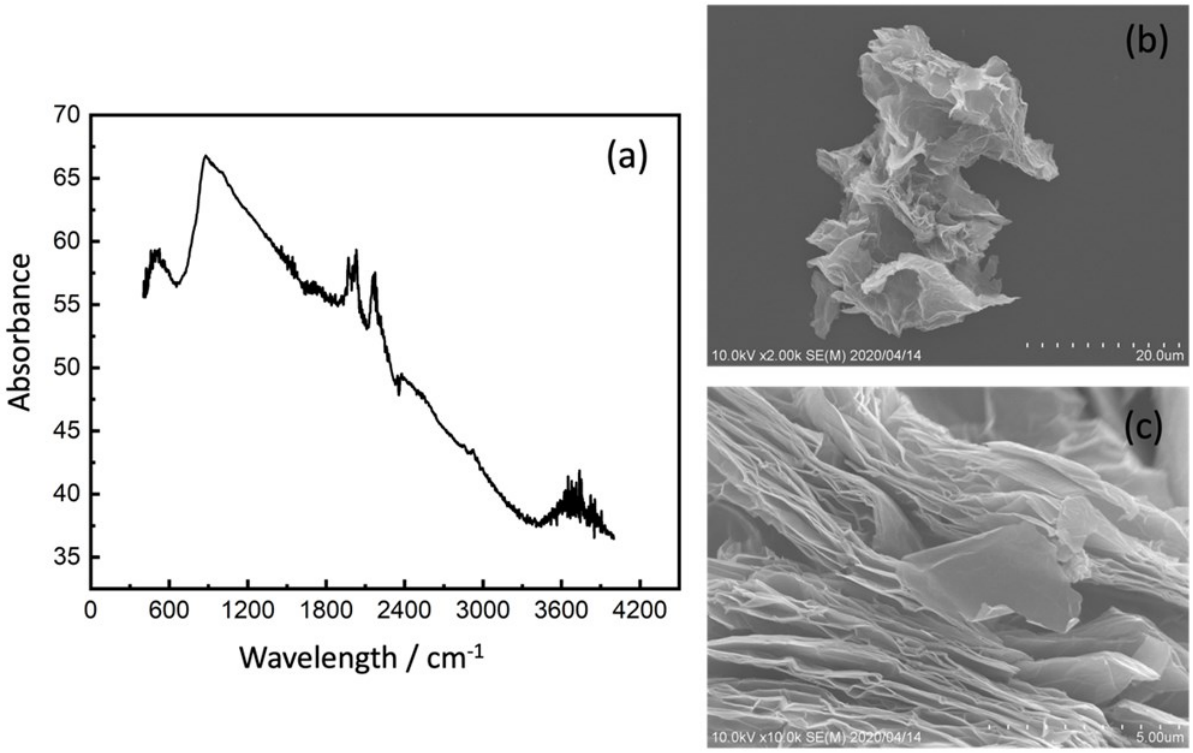

893 **Figure 5S**

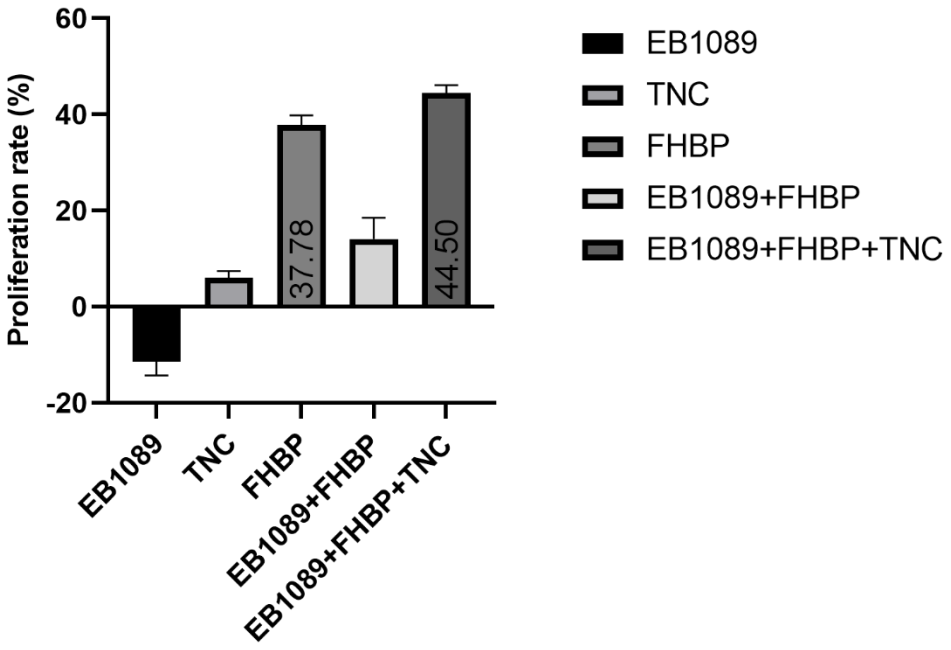

894

895

896 **Figure 6S**

897

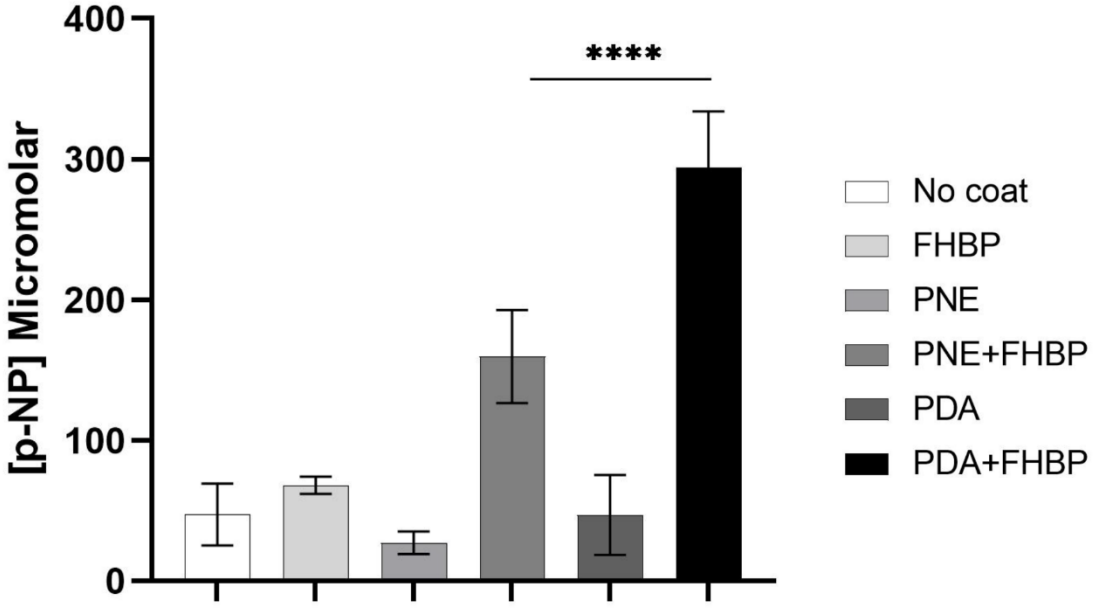

898

899

900

901 **Supplementary table1.** Sequence of Primers used.

902

903 **Supplementary table1:** Sequence of Primers used.

Gene	Forward	Reverse
Osteopontin	5'-AAGCGAGGAGTTGAATGG-3'	5'-CTCATTGCTCTCATCATTGG-3'
Osteocalcin	5'-CAGCGAGGTAGTGAAGAGAC-3'	5'-GCCAACTCGTCACAGTCC-3'
Collagen Type I	5'-CGGAGGAGAGTCAGGAAG-3'	5'-CAGCAACACAGTTACACAAG-3'
GAPDH	5'-GAAGGTGAAGGTCGGAGTC-3'	5'-GAAGATGGTGATGGGATTTC-3'

904

905

906

907

908

909

910

911

912

913

914

915

916

917

918

919

920

921

922

923

924 **Graphical abstract**

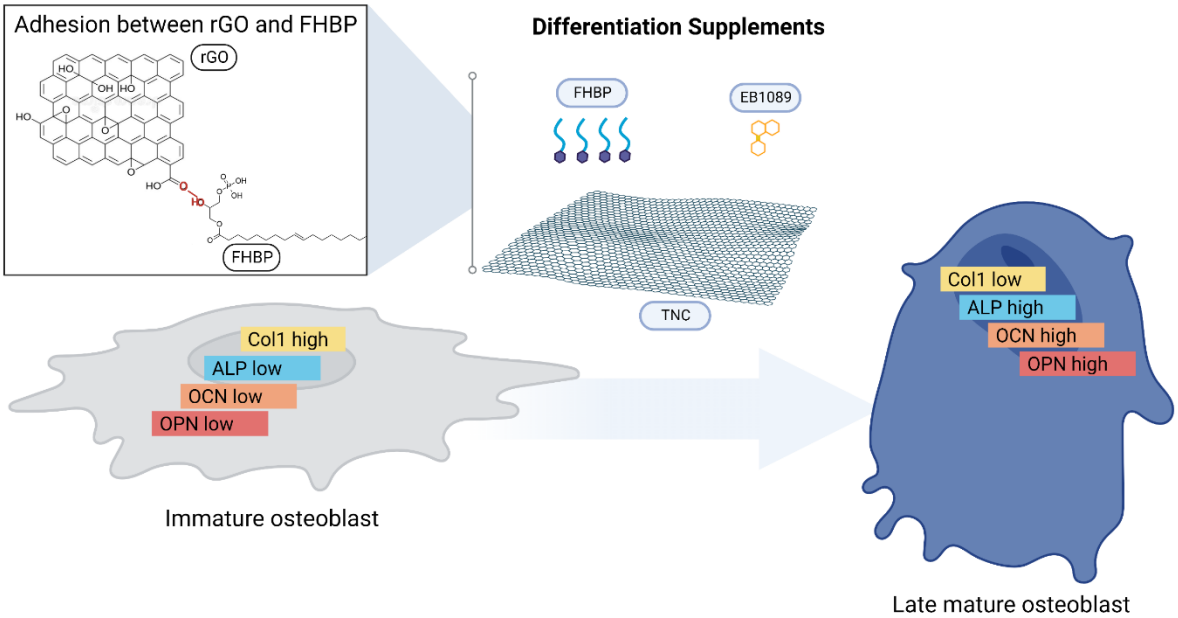
Adhesion between rGO and FHBP
rGO
FHBP
Differentiation Supplements
FHBP
EB1089
TNC
Col1 high
ALP low
OCN low
OPN low
Immature osteoblast
Col1 low
ALP high
OCN high
OPN high
Late mature osteoblast

Figure 1

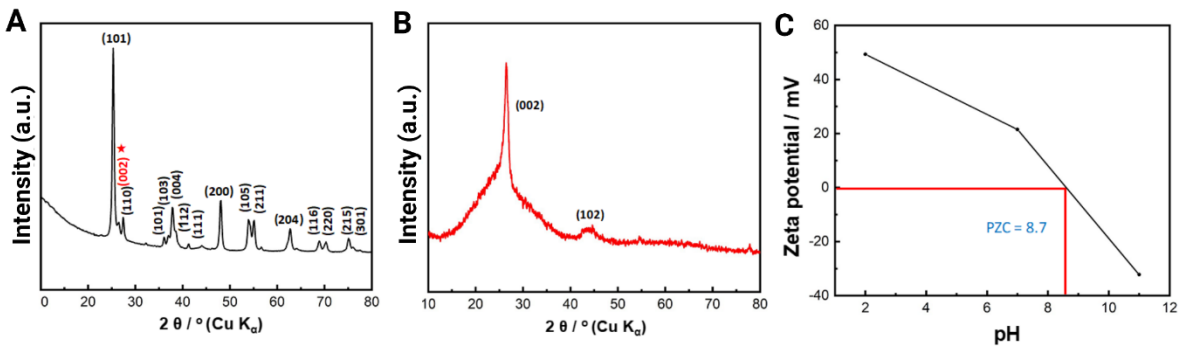

Fig. 2. XRD analysis of (A) TNC (P25/rGO/Ag nanocomposite), (B) rGO nanosheets and (C) Zeta potential at different pH of TNC.

Figure 2

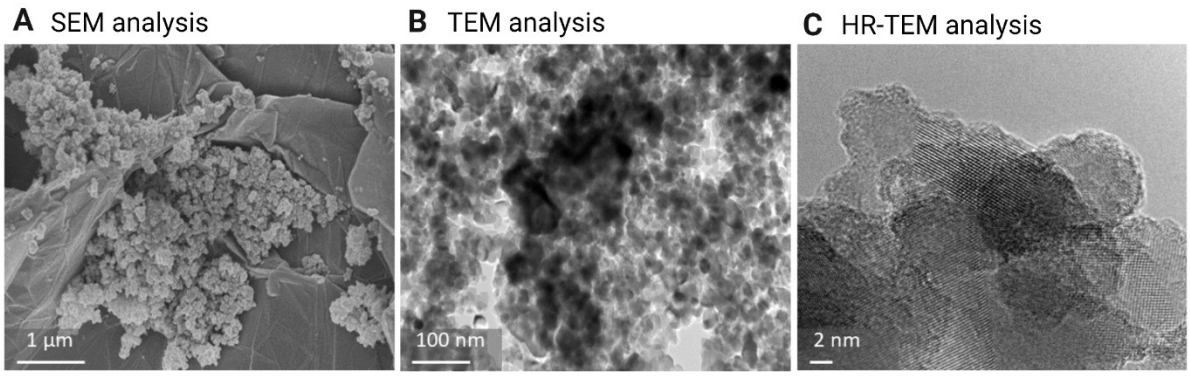

Fig. 2. A) SEM analysis B) TEM analysis, and C) HR-TEM analysis of TNC (P25/rGO/Ag nanocomposite.

Figure 3

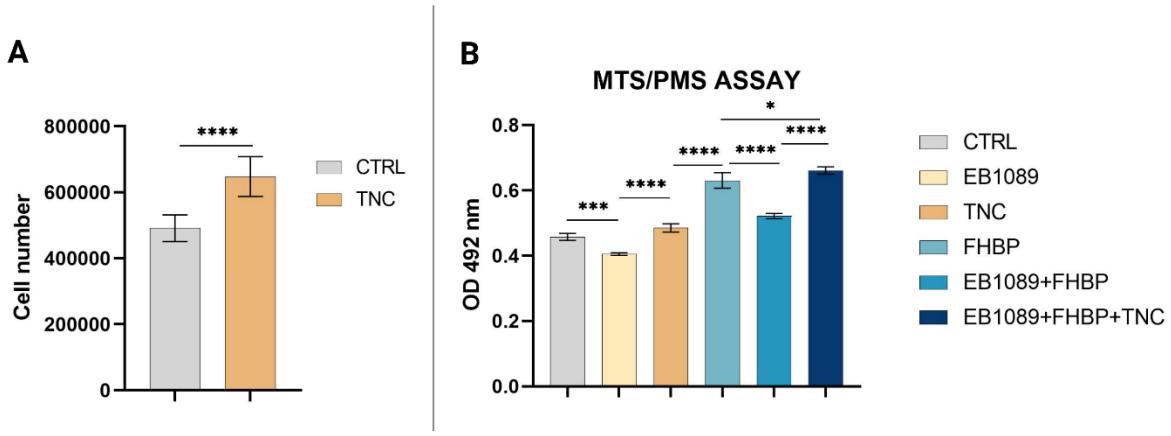

Fig. 3. Biocompatibility of TNC. (A) MG63 viability and cell growth in presence of TNC after 24 hrs. (B) MTS/PMS assay of MG63 after 3 days of culture with EB1089, FHBP, and TNC. Data are represented as the mean ± SD (*$p < 0.05$, ***$p < 0.001$ and ****$p < 0.0001$).

Figure 4

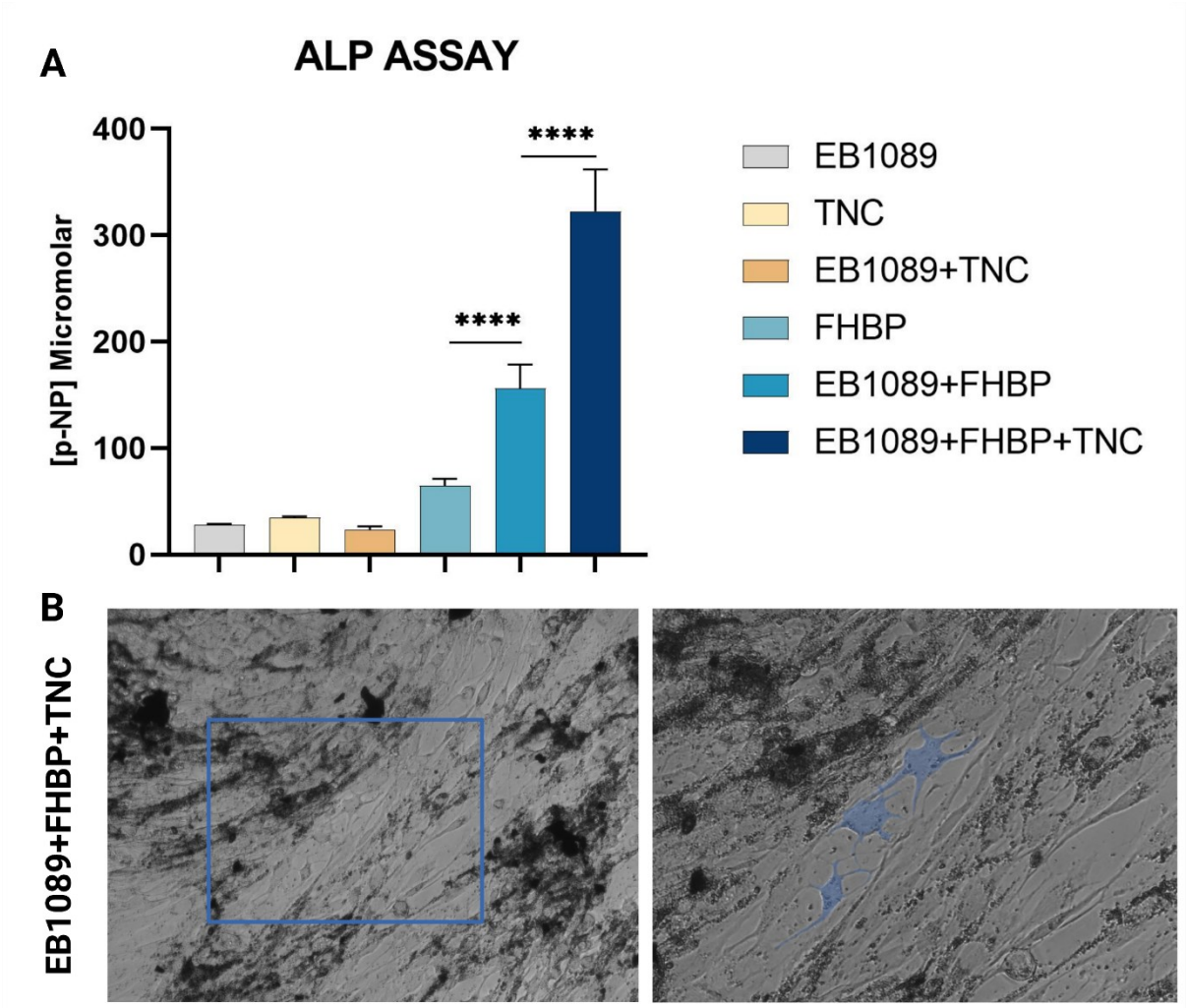

Fig. 4. TNC enhance MG63 maturation in presence of EB1089 and FHBP. A) Quantitative analysis of ALP activity, data are represented as the mean ± SD (****$p < 0.0001$). B) Morphological changes of MG63 in EB1089+FHBP+TNC group showing osteocyte-like cells with characteristic dendrites morphology as described by Blank and Sims 2019, 20x image, the cells were highlighted with blue colour.

Figure 5

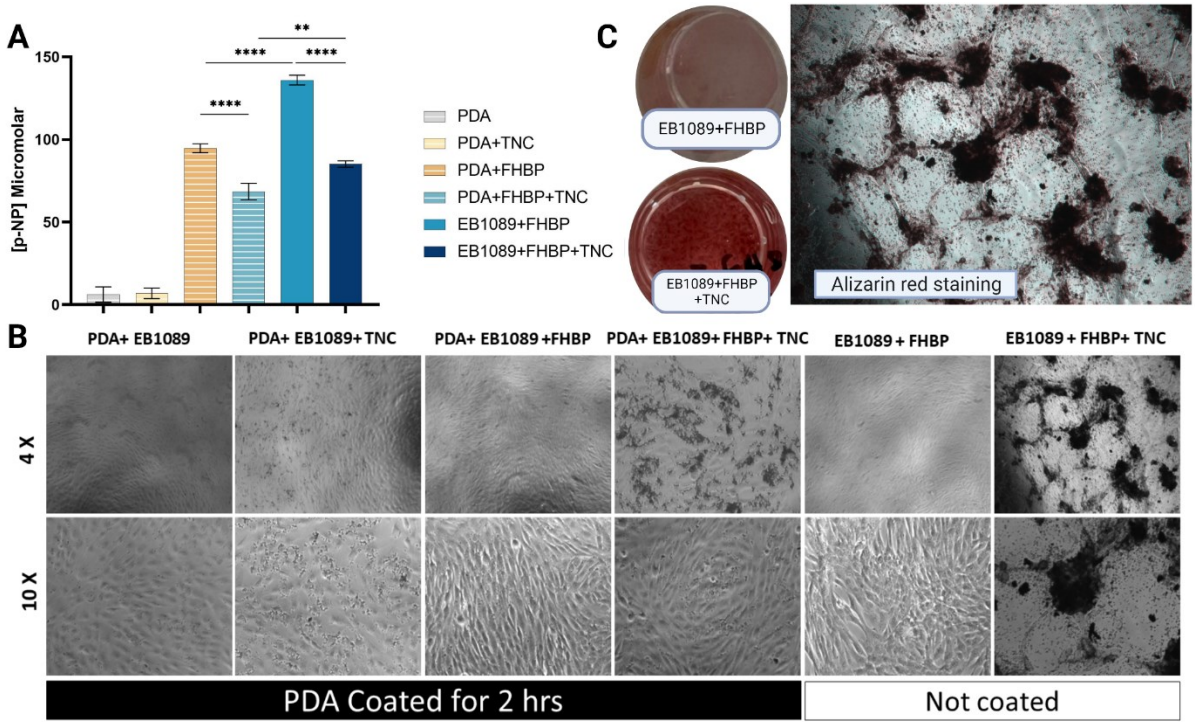

Fig. 5. Coating polystyrene plate with catecholamines. A) Assessment of TNC inclusion to EB1089+FHBP combination on MG63 maturation using ALP assay. Data are represented as the mean ± SD (**$p < 0.01$, and ****$p < 0.0001$). B) Representative images showing the morphological appearance of MG63 seeded at density of 120k on surfaces coated with EB1089, FHBP, TNC or combination of 2 or more of them with the aid of PDA. Also, uncoated groups treated with EB1089+FHBP with and without TNC were imaged. C) Alizarin red staining of MG63 (1.2×10^5 cells/mL/well) suspended in EB1089+FHBP+TNC showing cell aggregation after 3 days of culture in an uncoated regular well plate.

Figure 6

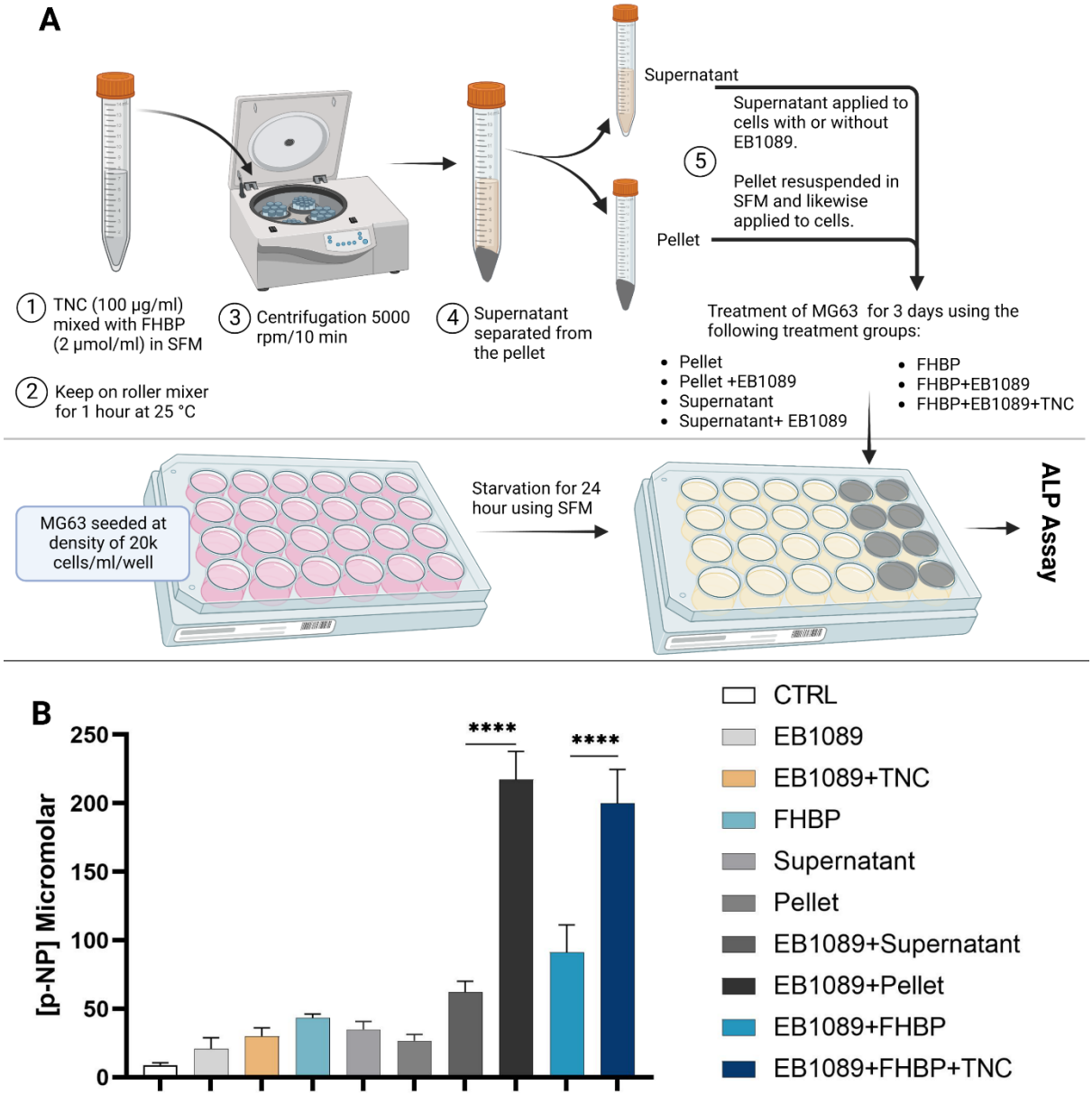

Fig. 6. Evidence for the binding of FHBP to TNC after stirring for 1 hour at 25 °C. A) Schematic diagram showing the experiment design. Created with BioRender.com. B) Quantitative analysis of ALP activity of MG63 in presence of supernatant and TNC pellet with and without EB1089. Groups treated with EB1089, FHBP, EB1089+FHBP, EB1089+FHBP+TNC as well as non-treated cells were included for better comparative evaluation. Data are represented as the mean ± SD (****$p < 0.0001$).

Figure 7

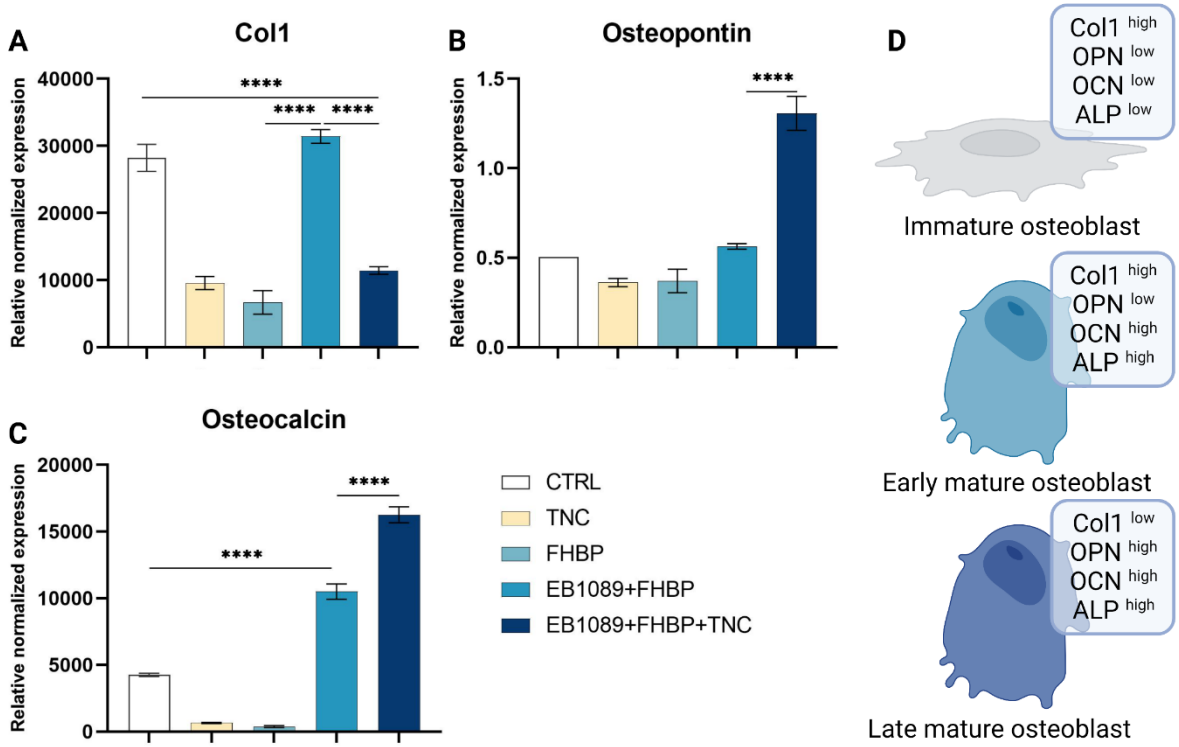

Fig. 7. Quantitative real-time polymerase chain reaction analysis. The expression levels of mRNAs A) collagen I (Col1), B) osteopontin (OPN) and C) osteocalcin (OCN) normalized to GAPDH in MG63 non-treated as control and treated with EB1089, FHBP, TNC and their combinations as determined by real-time qRT-PCR. The data are represented as the mean ± SD (****$p < 0.0001$). D) Schematic diagram showing cell maturation status based on mRNA expression as well as ALP analysis. Graph was created with BioRender.com

Figure 8

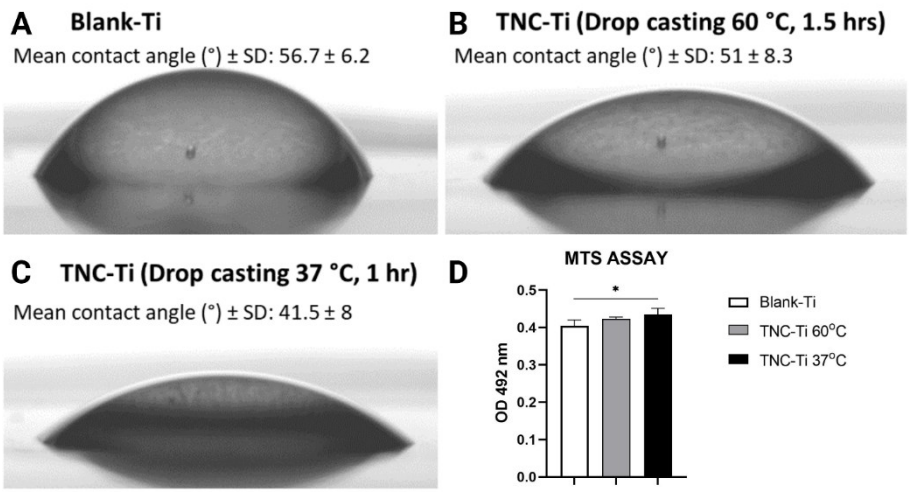

Fig. 8. Surface contact angle measurements of blank-Ti. (A) and TNC-Ti discs coated by drop casting at 60 °C (B) and 37 °C (C). (D) MTS/PMS assay of MG63 after 3 days of culture on the top of blank-Ti, TNC-Ti 60 °C and TNC-Ti 37 °C. Data are represented as the mean ± SD (*$p < 0.05$).